JACS
JOURNAL OF THE AMERICAN CHEMICAL SOCIETY

ARTICLE

pubs.acs.org/JACS

In Silico Partitioning and Transmembrane Insertion of Hydrophobic Peptides under Equilibrium Conditions

Jakob P. Ulmschneider,*[,†] Jeremy C. Smith,[†,‡] Stephen H. White,[§] and Martin B. Ulmschneider*[,§]

[†]IWR University of Heidelberg, Germany

[‡]Oak Ridge National Laboratory, Oak Ridge, Tennessee 37831, United States

[§]Department of Physiology & Biophysics, University of California at Irvine, Irvine, California 92697, United States

Supporting Information

ABSTRACT: Nascent transmembrane (TM) polypeptide segments are recognized and inserted into the lipid bilayer by the cellular translocon machinery. The recognition rules, described by a biological hydrophobicity scale, correlate strongly with physical hydrophobicity scales that describe the free energy of insertion of TM helices from water. However, the exact relationship between the physical and biological scales is unknown, because solubility problems limit our ability to measure experimentally the direct partitioning of hydrophobic peptides across lipid membranes. Here we use microsecond molecular dynamics (MD) simulations in which monomeric polyleucine segments of different lengths are allowed to partition spontaneously into and out of lipid bilayers. This approach directly reveals all states populated at equilibrium. For the hydrophobic peptides studied here, only surface-bound and transmembrane-inserted helices are found. The free energy of insertion is directly obtained from the relative occupancy of these states. A water-soluble state was not observed, consistent with the general insolubility of hydrophobic peptides. The approach further allows determination of the partitioning pathways and kinetics. Surprisingly, the transfer free energy appears to be independent of temperature, which implies that surface-to-bilayer peptide insertion is a zero-entropy process. We find that the partitioning free energy of the polyleucine segments correlates strongly with values from translocon experiments but reveals a systematic shift favoring shorter peptides, suggesting that translocon-to-bilayer partitioning is not equivalent but related to spontaneous surface-to-bilayer partitioning.

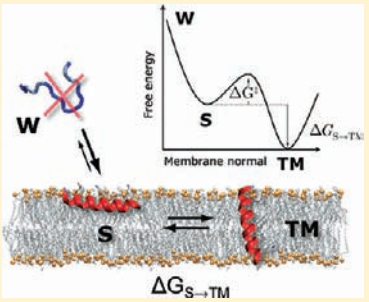

INTRODUCTION

The most fundamental stability principle of helix-bundle membrane proteins (MPs) is that the free energy of transfer of the constituent transmembrane (TM) helices must favor the membrane rather than the aqueous phase. This truism has resisted direct quantitation, because of the experimental challenges of measuring water-to-bilayer transfer free energies of hydrophobic peptides. Aggregation in the aqueous phase is the principal issue.[1,2] Cells have conquered this problem by means of the translocon machinery, consisting primarily of the SecY complex of membrane proteins in bacteria and archaea and the highly homologous Sec61 complex in eukaryotes. The SecY/Sec61 translocons receive nascent membrane chains directly from the ribosome and guide their insertion into the membrane cotranslationally. All available evidence suggests that the TM segments partition between the translocon complex and the lipid bilayer following physicochemical principles.[3−5]

Recent in vitro experiments have yielded the code that Sec61 uses for selecting nascent chain segments for insertion into the bilayer.[3,4] The code, in the form of a biological hydrophobicity scale, is highly correlated with physical hydrophobicity scales determined, for example, from measurements of the partitioning of amino acids between water and *n*-octanol.[6] Nevertheless, no direct quantitative comparison of water-to-bilayer and translocon-to-bilayer free energies of TM helices has been possible because of the insolubility of model segments in the aqueous phase. As discussed by Schow et al.,[7] a quantitative comparison is necessary for completing our understanding of the translocon-to-bilayer partitioning process, and for connecting membrane protein stability to translocon-guided membrane protein assembly. To circumvent the experimental challenges of partitioning transmembrane segments across lipid membranes, we have adopted a computational approach using molecular dynamics (MD) simulations carried out in the microsecond time regime. Because the simulations use the same TM segments used in a recent in vitro study of the translocon-assisted insertion of polyleucine segments of various lengths,[8] it was possible to compare direct peptide partitioning with translocon-to-bilayer partitioning.

Our simulations use microsecond-scale equilibrium MD simulations to measure and quantify the transfer properties of monomeric peptides into lipid bilayers: sequences are allowed to transition spontaneously into and out of the lipid bilayer membrane, thus providing the true thermodynamic partitioning equilibrium. The strength of this partitioning approach is that all

Received: May 2, 2011
Published: August 23, 2011

states populated at equilibrium are directly detected, and the free energy between them is obtained from their relative occupancies. Like an equivalent laboratory experiment, this approach is completely unbiased. No positional or conformational restraints, or umbrella potentials, are applied, and the results do not depend on the initial peptide conformation or location. Furthermore, the method yields the insertion kinetics as well as the atomic-resolution structural dynamics of the partitioning process. The resulting insertion propensities thus reflect only the strength of the peptide−bilayer interactions. We show that a single MD simulation of 1−2 μs is usually sufficient to obtain the free energy of insertion from the ratio of TM embedded to noninserted populations.

Microsecond-length simulations can now be performed routinely using advanced MD programs such as Gromacs (www.gromacs.org) or Hippo (www.biowerkzeug.com). These methods exploit fully the single instruction, multiple data (SIMD, SSE) architectures of modern multicore x86 CPUs. These programs typically achieve speeds of 30−50 ns per day, without any compromise in accuracy compared to other MD software. As an example, the 1 μs partitioning simulations performed in this paper take 1−2 months on a single modern Intel/AMD CPU. Larger systems can generally achieve similar speeds but require more CPUs.

In order to compare the simulations with translocon-based partitioning, we concentrate in this study on a set of polyleucine peptide (Ln) constructs that have previously been studied experimentally.[8] These systems have the convenient property that the partitioning equilibrium can be shifted from TM inserted to noninserted by shortening the peptide. In the translocon experiments, the insertion free energy as a function of peptide length n can be fitted to a simple linear function $\Delta G(n) = n\Delta G_{Leu} + \Delta G_0$, indicative of a two-state equilibrium model. We show here that direct insertion closely follows this model but with a constant offset with respect to the translocon data.

RESULTS

Partitioning Pathway. We have obtained the partitioning properties of two polyleucine constructs: (i) unflanked acetyl-$(L)_n$-amide constructs (Ln), and (ii) flanked acetyl-GGPG-$(L)_n$-GPGG-amide peptides (GLn), with n = 5−12. The GLn sequences were used in the translocon assay, with the GGPG flanks serving as helix breakers, insulating the polyleucine 'guest' segments from the host sequence.[8] All-atom MD simulations of the peptides were carried out in palmitoyloleoyl-phosphatidylcholine (POPC) lipid bilayers, with a length of 1−2 μs per run (see Table S1 in Supporting Information for a complete list of simulations performed). Simulations are generally performed at elevated temperatures ($T \geq 80$ °C), as this greatly speeds sampling.[9] We show below that the thermodynamic properties of the systems are independent of temperature, even for very hot systems (>200 °C).

The free partitioning of hydrophobic peptides into lipid bilayers is schematically illustrated in Figure 1A. The two principal states are a surface-bound helix (S) and a transmembrane-inserted helix (TM). Water-solvated states (W) are much higher in free energy and not populated at equilibrium. This is consistent with experiments that show these peptides precipitate out of solution.[1,2] Thus, as demonstrated further below, the partitioning for these peptides takes place between S and TM states, rather than between water and TM. For comparison,

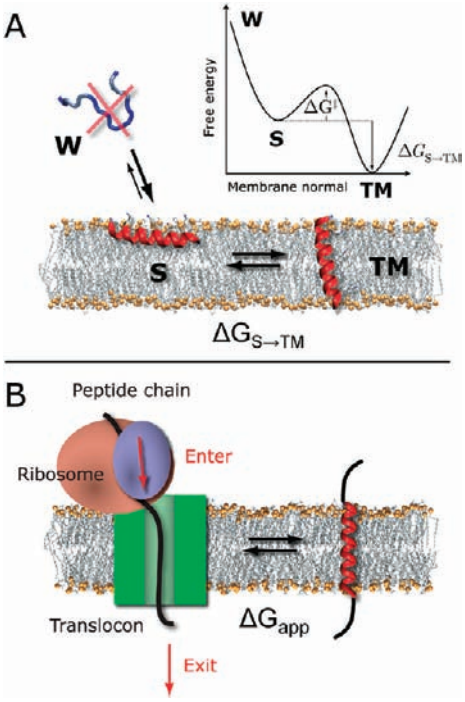

Figure 1. (A) Schematic partitioning equilibrium for peptides that are sufficiently hydrophobic to insert autonomously into membranes ($\Delta G_{S\to TM}$). Only two states are populated at equilibrium: an α-helix located either on the membrane surface (S) or transmembrane-inserted (TM). Water-soluble states (W) are not populated, consistent with the experimental fact that these peptides precipitate out of solution. (B) Schematic depiction of the translocon−bilayer partitioning equilibrium presumably probed by the translocon-mediated insertion experiments (ΔG_{app}). The entry of the peptide into the translocon ("Enter") and subsequent secretion ("Exit") are thought to be nonequilibrium processes.

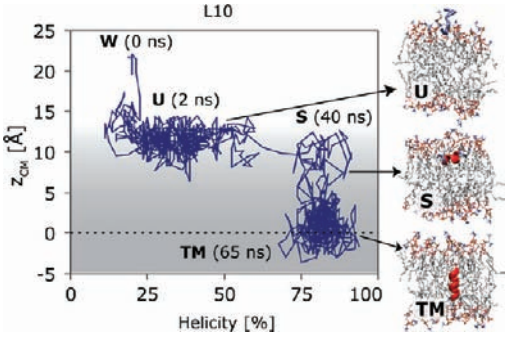

Figure 2. Illustration of the fast folding and adsorption process from the initial water-solvated unfolded state (W). The insertion depth z_{CM} is plotted versus the peptide helicity for the pathway taken by L10 at 80 °C. Interfacial adsorption from the initial state in water occurs in ~2 ns (U). The peptide then folds (S) and subsequently inserts (TM). All other studied sequences behave exactly similar. Only the S and TM states are observed for the remainder (1−2 μs) of the simulations.

Figure 1B depicts the process assumed to be probed by the translocon-mediated insertion experiments.[3−5] Recent simulations as well as experiments indicate this likely represents an equilibrium partitioning process of peptides between translocon channel and bilayer, rather than between water-soluble and TM states (see Discussion below).[7,10−14] In this model, the entry of

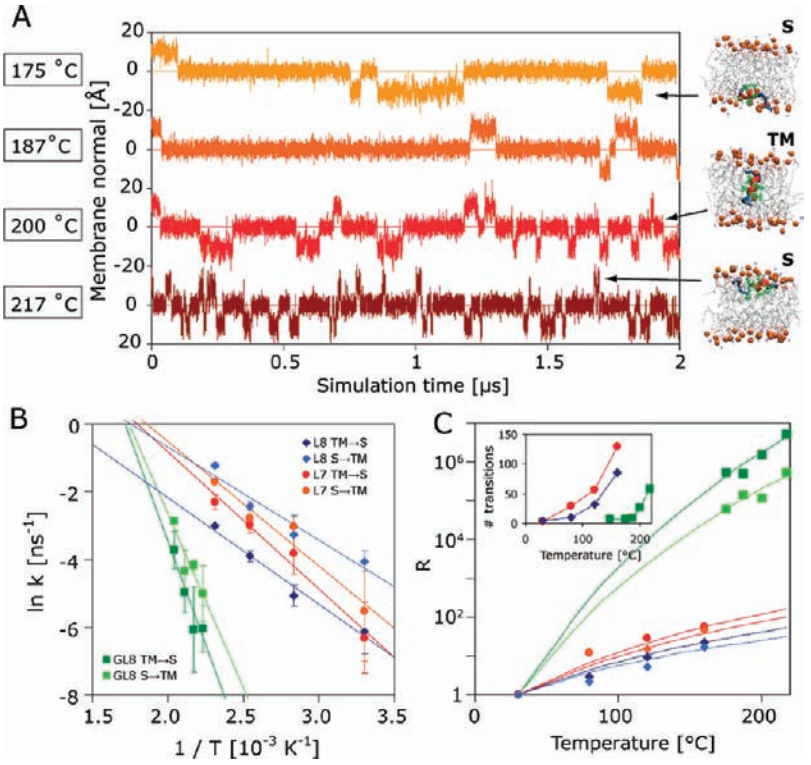

Figure 3. Temperature dependence of the partitioning kinetics: (A) A plot of the center of mass (z_{CM}) position of the peptide (here GL8) along the membrane normal shows multiple transitions between S (z = ~12 Å) and TM (z = 0 Å) states. The number of transitions rises rapidly as the temperature is increased (inset, panel *C*). (B) Arrhenius plots of the insertion and expulsion rates (shown are L7, L8, and GL8) all exhibit single-exponential kinetics. Flanked peptides have much larger barriers (slope of fit; cf., L8 and GL8). Consequently, the temperature has to be raised by ~100−150 °C to observe partitioning events in the 2 μs GL*n* simulations. The Arrhenius plot allows extrapolation of the insertion and expulsion times to room temperature. For example, GL8 has a predicted insertion time of $\tau_{S\rightarrow TM} \approx 9$ ms at 30 °C, which is ~10^5 times slower than at 217 °C. (C) The partitioning rate increase R over ambient temperatures shows rapid growth with respect to temperature. This effect is much smaller for unflanked peptides, where the insertion barrier is weaker.

the peptide into the translocon ('Enter') and the translocation ('Exit') are energetically driven and nonequilibrium.

The typical peptide insertion pathway observed in the simulations is shown in Figure 2. All peptides were initially unfolded and placed into bulk water about 15 Å from the bilayer surface (W). Rapid adsorption (U) at t = 5−10 ns, consistent with insoluble hydrophobic peptides, is followed by interfacial folding into a surface-bound helix (S). Subsequently the peptides insert and adopt a TM helix orientation. This pathway agrees well with the thermodynamic models of White[15] and Engelman,[16] in which folding precedes insertion. The adsorption process was irreversible in all simulations, with no subsequent expulsion of the peptide into the water phase (W), or unfolded conformations (U) observed after ~50 ns. Only the α-helical S and TM states remained for the following 1−2 μs (Figure 3). The initial 50 ns of every simulation were thus considered the equilibration period and dropped from further analysis. After t > 50 ns, the simulations are in the 'equilibrium' phase, characterized by frequent transitions between α-helical S and TM states (Figure 3). These can be distinguished by their characteristic center-of-mass position along the membrane normal (z_{CM}) and the helix tilt angle (θ). The TM state is deeply buried in the center of the bilayer and aligned along the membrane normal ($z_{CM} \approx 0$ Å, $\theta \approx 10°$), whereas the S helix is parallel to the membrane surface ($z_{CM} \approx 12$ Å, $\theta \approx 90°$). The density profile of the S-state (Figure 4A) reveals the peptide to be deeply buried near the edge of the acyl chains, just below the glycerol/carbonyl groups (Figure 4A). The S position substantially deforms the monolayer surface containing the peptide, with up to ~2.5 Å local thinning through the disturbance of the lipids (Figure 4B). However, water is not pulled into the bilayer in significant numbers by the peptide, as can be seen by the water density curve that is essentially identical to that of the opposing interface. For short peptides ($n \leq 6$), S configurations dominate, while longer polyleucine segments ($n \geq 10$) mainly insert to form TM helices. Peptides of intermediate lengths (n = 7−9) display an equilibrium alternating between S and TM configurations.

Peptide and Bilayer Thermostability. To obtain multiple partitioning events within the ~2 μs simulation time frame, the temperature was elevated to accelerate sampling in many of the simulations (Table S1). The use of high temperatures in simulations is now widespread through replica exchange ensemble simulations (REMD),[17] and such simulations have also been previously performed to study peptide−membrane partitioning phenomena.[18−24] For the approach taken here, it is required that the equilibrium properties of the peptide and bilayer do not change upon heating (see also Temperature Insensitivity of the Partitioning Propensities below). The key property influencing the partitioning free energy is the secondary structure of the peptide, which must not denature upon heating. As shown in Figure 5B for L8, L12, and GL12, there is no significant loss of helicity (<10%) upon raising the temperature from 30 to 217 °C.

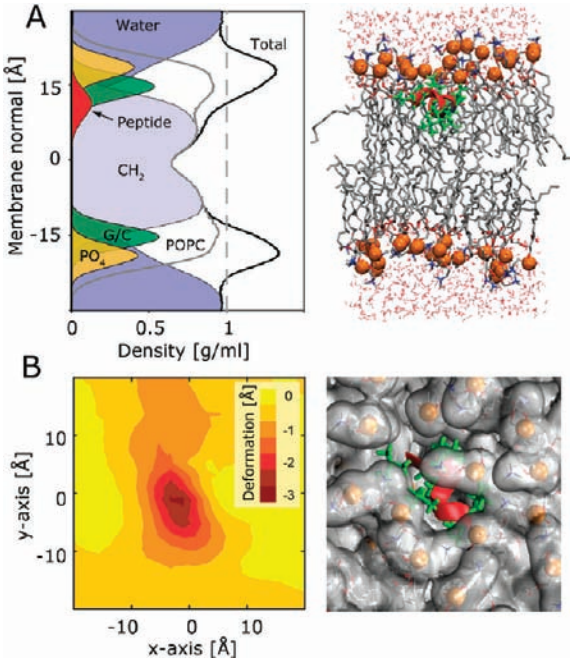

Figure 4. Peptide location and bilayer deformation of the interfacial surface-bound (S) state of L*n* and Gl*n* peptides: (A) the density cross-section profile of the bilayer shows that in the S state the peptide (here L7) is buried below the water interface. A representative conformer is shown to scale. The leucine side chains (green) are chiefly in contact with the acyl tails (CH_2), and there is only a small overlap with the phosphocholine headgroups and carbonyl-glycerol (C/G) groups. Other peptides behave exactly similar. (B) The peptide-induced distortion to the bilayer at equilibrium can be visualized by plotting the time-averaged phosphate position from the bilayer center. This shows local thinning by 5−10% for L7 as the lipid headgroups bend over the peptide to cover the termini (phosphate is represented as an orange sphere).

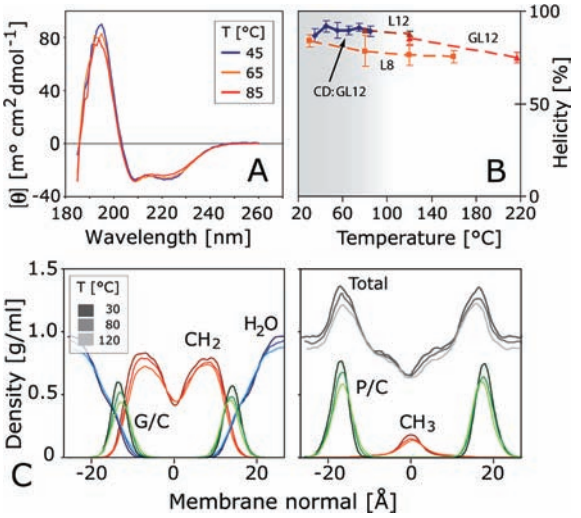

Figure 5. Thermostability of the peptide and bilayer: (A) circular dichroism spectra of the secondary structure of GL12 in POPC vesicles (peptide/lipid ratio = 1/100) over a temperature range of 45 °C to 85 °C. The spectra indicate predominantly helical conformers and display low sensitivity to temperature. (B) The thermostability of the peptides observed in the MD simulations is comparable (shown are L8, L12, and GL12; all other peptides behave similar). Shorter peptides are marginally less helical due to terminal fraying. (*C*) The effect of heating on the lipid bilayer can be visualized by plotting the equilibrium trans-bilayer density profiles in the presence of peptide (here L8) for temperatures in the range 30−120 °C (dark to light colors). Comparison of the principal structural groups (CH_3 = methyl, CH_2 = acyl tails, P/C = phosphocholine headgroups, G/C = carbonyl-glycerol linker, H_2O = water) shows temperature-induced broadening of the Gaussians and a slight decrease in the total density. However, the trans-bilayer density profile and location of the principal structural groups does not change significantly.

In contrast, the GPGG flanks remain entirely unstructured at all temperatures (Figure S1), consistent with the low helicity of glycine and proline residues. The thermostability was confirmed experimentally using circular dichroism spectroscopy (CD). Spectra of GL12 peptides embedded in DPPC vesicles are shown in Figure 5A. Heating from 45 °C to 85 °C did not decrease peptide helicity, and no melting transition was observed. These results are consistent with recent experimental findings that hydrophobic membrane-inserting peptides display exceptional thermostability. CD spectra of tryptophan-flanked hydrophobic core peptides (WALP) incorporated into synthetic bilayers (DMPC, DPPC and DOPC), or 1-octanol, showed that the peptides were fully helical, even at 90 °C.[9] The principle cause is the deep burial of the peptides in the hydrophobic membrane core, where the penalty of exposing unmatched backbone hydrogen bonds is too severe (~4 kcal/mol per peptide bond) to allow thermal unfolding.[25,26] This applies also to the S state, which is observed to be at the edge of the hydrophobic region (Figure 4).[9]

The physiochemical properties of the lipid bilayer also do not seem to change dramatically upon heating (Figure 5C). The cross-sectional density profile of a POPC bilayer reveals a broadening of the Gaussians associated with the principal structural groups upon thermal expansion. The membrane also thins slightly (~5% at 120 °C), and the area per lipid increases. However, the relative positions of key groups along the membrane normal do not change, and the overall chemical and hydrophobicity profile of the bilayer is maintained. Experimental measurements on the thermostability of lipid membranes indicate that bilayers are stable at high temperatures: for example, grazing angle neutron scattering measurements on POPC multilamellar vesicles reveal stable bilayers even up to a temperature of 115 °C.[27] More experimental data on the high-temperature behavior of lipid bilayers will be required to investigate whether the simulation results at the highest temperatures are reliable. However, there is no obvious reason why the lipid parameters that were properly parametrized in the range of 0−50 °C should fail entirely under hotter conditions (50−150 °C).

While the simulation temperature can be raised up to ~225 °C, results for T > 100 °C do not resemble real-world behavior and are used here solely as a convenience to speed sampling. Experiments at T > 100 °C would result in the water boiling off at 1 bar pressure. This is not observed in the MD simulations due to the use of liquid-state isothermal−isobaric (NPT) pressure and temperature coupling algorithms that cannot sustain vapor/liquid coexistence. Simulating the correct boiling behavior of the water model requires the dedicated modeling of a liquid−vapor interface through, for example, Gibbs ensemble methods.[28,29] However, the high-temperature simulations in the range T = 100−210 °C are still useful, because heating affects the partitioning kinetics but not the thermodynamics (i.e., ΔG of insertion), as shown below. The limit of this convenient technique to speed sampling is reached at $T \approx$ 225 °C, at which point the simulations become unstable.

Table 1. Partitioning Kinetics of the L7, L8, and GL8 Peptides[a]

	L7	L8	GL8
$\Delta H^{\ddagger}_{S\rightarrow TM}$ (kcal/mol)	7.3 ± 3	5.5 ± 2	20 ± 6
$\Delta H^{\ddagger}_{TM\rightarrow S}$ (kcal/mol)	8.1 ± 3	6.3 ± 2	24 ± 7
$\tau_{S\rightarrow TM}$ (T = 30 °C)	250 ± 183 ns	58 ± 17 ns	9 ± 3 ms
$\tau_{TM\rightarrow S}$ (T = 30 °C)	551 ± 245 ns	457 ± 162 ns	226 ± 90 ms

[a] The barrier heights $\Delta H^{\ddagger}$ are obtained from the slope of the Arrhenius plots. Transition times τ for L7 and L8 are from averaging at 30 °C. τ for GL8 is derived by extrapolating the Arrhenius plot to 30 °C. Error estimates are from averaging over 10 blocks.

Insertion Kinetics. The effect of higher simulation temperatures is a dramatic increase in the peptide insertion and expulsion rates. This is illustrated in Figure 3 and Table 1 for GL8. As the temperature is raised from 175 °C to 217 °C, the peptide transits much more frequently between the TM and S states (Figure 3A). Average insertion and expulsion rates, k_{in} and k_{out}, can be computed from these simulations. The resulting kinetics are summarized (for L7, L8, and GL8) as an Arrhenius plot in Figure 3B. In all cases, a fit of ln k versus $1/T$ results in a straight line, indicating a first-order, single-barrier process. From the slope of the fit, the activation enthalpies for both insertion and expulsion $\Delta H^{\ddagger}$ can be estimated via $\ln k = -\Delta H^{\ddagger}/RT$ + constant (Table 1). The barriers for both L7 and L8 are quite weak, with $\Delta H^{\ddagger} \sim 5-8$ kcal/mol and transition times of up to ~0.5 μs at 30 °C. However, the situation is very different for GL8, with vastly increased barriers of $\Delta H^{\ddagger} \sim 20-24$ kcal/mol. No transition events were observed on the 2 μs scale unless the system was heated to ~140 °C. It is possible to obtain the insertion and expulsion rates at 30 °C by extrapolating the Arrhenius plot. This gives $\tau \approx 9-226$ ms, roughly $\sim 10^6$ times slower than for L8, which is certainly beyond the time scales that can currently be reached in simulations. The cause of the slower rate for GL8 is the barrier for translocating one GPGG flanking tetrapeptide that strongly resists burial in the membrane interior. As the flanking sequence tends to be unfolded, this would expose unpaired backbone hydrogen bonds to the hydrophobic membrane interior, which is energetically highly disfavored.

The combination of high peptide thermostability and greatly accelerated partitioning kinetics allows the simulation temperature to be used as a simple tool to dramatically speed partitioning events. Plotting the ratio of high temperature to room temperature rates (Figure 3C) shows that an increase from 30 °C to 160 °C results in 9−40 times faster kinetics for L7 and L8. For GL8, the increase from 175 °C to 217 °C results in about 9 times faster kinetics; extrapolation to 30 °C suggests an immense factor of $\sim 4 \times 10^5$. Thus, a simple increase in simulation temperature enables the study of peptide partitioning phenomena that would be unfeasible at room temperature.

Partitioning Equilibrium. The thermodynamic partitioning equilibrium can be visualized by projecting the free energy ΔG as a function of the peptide tilt angle θ and center of mass position z_{CM} along the membrane normal (Figure 6). The surfaces have three minima, one for the characteristic TM position at $z_{CM} \approx 0$ Å, $\theta < 30°$ and two for the S state at $z_{CM} = \pm 12-14$ Å, $\theta > 70°$. For both series, there is a continuous shift from the S to the TM free energy minimum as the peptide length is increased from 5 to 10 leucines. For a given n, the Ln and GLn surfaces are surprisingly similar, with the same relative populations of TM and S states.

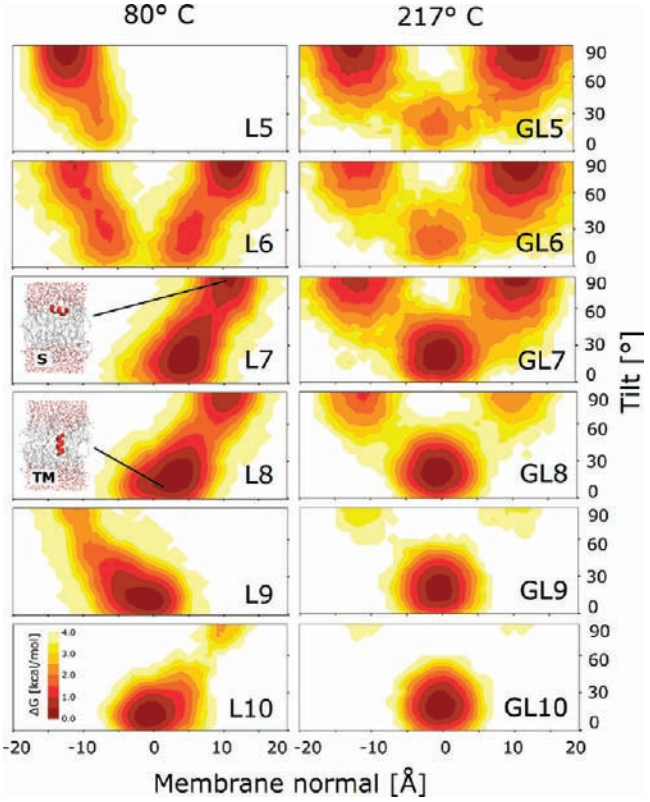

Figure 6. Two-dimensional free energy projection for the Ln (80 °C) and GLn (217 °C) peptides (n = 5−10) as a function of the position along the membrane normal (z) and tilt angle (θ). The surfaces reveal two distinct minima; one for TM-inserted and one for surface-bound peptides. For short peptides ($n \leq 7$), the interfacial S state ($z \approx 12$ Å, $\theta \approx 90°$) dominates, while longer peptides ($n \geq 8$) are preferentially TM-inserted ($z \approx 0$ Å, $\theta \approx 20°$). For a given peptide length n, the surfaces of unflanked Ln and GGPG-flanked GLn peptides are very similar, despite the different temperatures, demonstrating ΔG is chiefly determined by the number of leucines n. At 80 °C, the Ln runs are not fully converged. Heating to 120 °C results in full convergence, similar to the GLn simulations at 217 °C. The values of ΔG have been shifted so that the lowest bin is set to zero.

For symmetry reasons, the averaged ensemble populations of the two S minima should be identical. This was always the case for the GLn simulations, as the higher temperature allowed the peptide to cross the bilayer center repeatedly. The translocation barrier was not always overcome in the 80 °C simulations of Ln, indicating that these simulations are not yet fully converged. However, this can be overcome by increasing the temperature further to 120 °C or 160 °C (see Figure 8). For very short Ln peptides ($n \leq 7$), strong negative mismatch led to a shift of the TM minimum higher up into one bilayer leaflet, resulting in a broader TM minimum as the helix diffused along the membrane normal.

Given that there are only two states, the free energy difference assumes the simple equation $\Delta G_{S\rightarrow TM} = +kT \ln(1/p_{TM} - 1)$ characteristic of a two-state Boltzmann system, where p_{TM} is the probability of the TM state. It has been shown that the experimental insertion propensity p_n, as a function of the number of leucine residues n, can be fitted perfectly by the sigmoidal function $p_n = [1 + \exp(-\Delta G_n/kT)]^{-1}$.[8] Figure 7 shows the experimental and computed insertion propensities together with

dx.doi.org/10.1021/ja204042f | J. Am. Chem. Soc. 2011, 133, 15487–15495

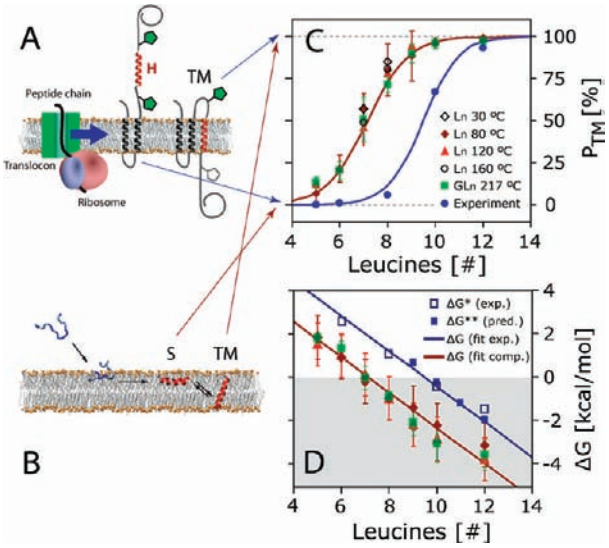

Figure 7. Bilayer insertion efficiency and transfer free energy as a function of peptide length *n*. (A) The experimental values are for translocon-mediated insertion into dog pancreas rough microsomes of GGPG-$(L)_n$-GPGG constructs embedded into the leader peptidase carrier sequence.[8] (B) The computed values are for spontaneous partitioning of L*n* peptides into POPC lipid bilayers at 30−160 °C, and for GGPG-$(L)_n$-GPGG at 217 °C. (C) Both measurements display perfect two-state Boltzmann behavior ($R^2 > 0.99$), with a transition in the native state from surface-bound to TM-inserted upon lengthening of the peptide. (D) This is reflected in the free energy of insertion $\Delta G(n)$ as a function of peptide length *n* (insertion for negative ΔG, shaded). The straight lines indicate the two-state Boltzmann fit, while the data points show the computed (red, green) and experimental (blue) values for the individual peptides (*measured ΔG,[4] peptide IDs: 43 and 380−383; **predicted ΔG, http://dgpred.cbr.su.se/).

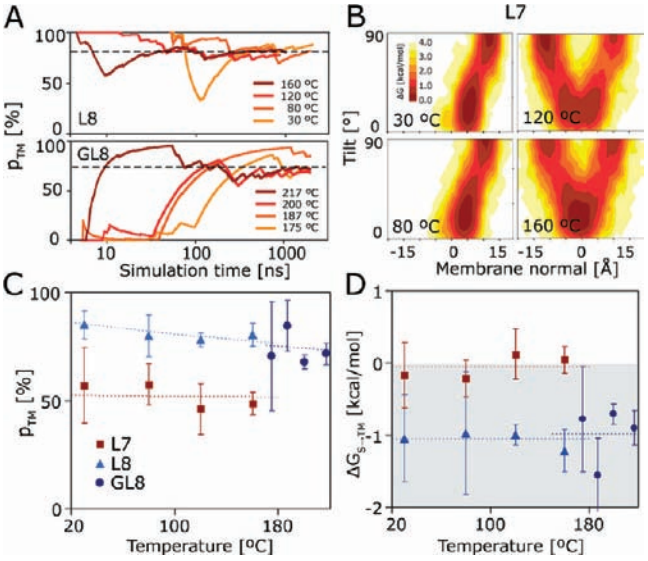

Figure 8. Temperature dependence of the insertion propensities p_{TM} and the transfer free energies $\Delta G_{S\to TM}$. (A) Convergence can be visualized by plotting a running average of p_{TM} against simulation time (note the logarithmic time-axis). Higher temperatures accelerate convergence toward the equilibrium (dashed line), which is independent of the starting configuration (here: TM for L8, S for GL8). (B) Free energy plots of the L7 peptide for 30−160 °C. Full convergence is seen at 120 °C and 160 °C, while the S-state is being populated in only one interface at 30−80 °C due to incomplete sampling. (C) Overall insertion propensities for L7, L8, and GL8 as a function of temperature. Error bars are derived from block averaging (10 blocks). (D) The corresponding free energies of insertion $\Delta G_{S\to TM}$ appear to show no systematic variation with temperature.

the best-fit models ($R^2 > 0.99$). All curves display two-state behavior, with a transition to TM-inserted configurations for longer peptides. Interestingly, the simulation-derived curves vary little with the temperature and/or the addition of the flanking sequences. Figure 7B shows that ΔG_n decreases perfectly linearly with *n* in both simulation and experiment. However, the offset and slope vary slightly, reflecting a shift of the MD insertion probability curve toward shorter peptides by ∼2.4 leucine residues, corresponding to a $\Delta\Delta G = \Delta G_{translocon} - \Delta G_{direct} = 1.9 \pm 0.1$ kcal/mol offset between the experimental and computational insertion free energies. This offset is a constant for all peptides.

Temperature Insensitivity of the Partitioning Propensities. A surprising result from these simulations is the low sensitivity of p_{TM} and $\Delta G_{S\to TM}$ to temperature. The insertion profiles at 80 °C and 120 °C are nearly indistinguishable (Figure 7). To investigate this further, we performed a scan (2 μs each) at four different temperatures for L7 and L8 (30−160 °C) and GL8 (147−217 °C). The resulting values of p_{TM} and $\Delta G_{S\to TM}$ are shown in Figure 8C and 8D. Although the statistical fluctuations are relatively large at the lower temperatures, there is no pronounced systematic effect. At the lowest temperatures of 30 °C and 80 °C, some of the L*n* simulations are not converged and sample only one interface. This adds an error of $-kT \ln 2$ to the estimate of $\Delta G_{S\to TM}$ (∼0.4 kcal/mol at 30 °C). Even after 2 μs, the statistical errors at these temperatures are significant due to the low number of transition events. Despite these uncertainties, the values of $\Delta G_{S\to TM}$ are similar to those at the higher temperatures, where convergence is achieved. To check whether the averages of p_{TM} are reliable, we calculated logarithmic convergence plots of p_{TM} as a function of simulation time (L8 and GL8, Figure 8A): p_{TM} is well converged at the higher temperatures and is independent of the starting conformation (S or TM). As expected, convergence proceeds much more rapidly as the system is heated. The observed thermodynamic behavior of the partitioning process best fits a model in which $\Delta G(T)_{S\to TM} \approx$ constant, and entropic contributions are small ($\Delta S_{S\to TM} \approx 0$), as shown in Figure 8C,D.

DISCUSSION

The poly-Leu insertion propensities derived from the simulations closely mimic those of the Sec61 in vitro assay (Figure 7) but reveal a systematic shift toward the TM state. At least 10 leucines are required for TM insertion in the experiments, whereas the simulations predict that sequences as short as eight leucines can insert. Interestingly, flanking sequences do not affect the insertion propensity, with almost identical results for $(L)_n$ and GGPG-$(L)_n$-GPGG (Figure 6, Figure 7). Given the eight additional flanking residues of the GL*n* peptides, and the very different simulation temperatures (80 °C vs 217 °C), this would seem at first surprising. However, a possible explanation arises from the structural properties of the flanks, which were specifically designed to remain unfolded through the use of Gly and Pro residues (Figure S1 (Supporting Information)).[3] The high cost of partitioning unmatched polar backbone groups into the

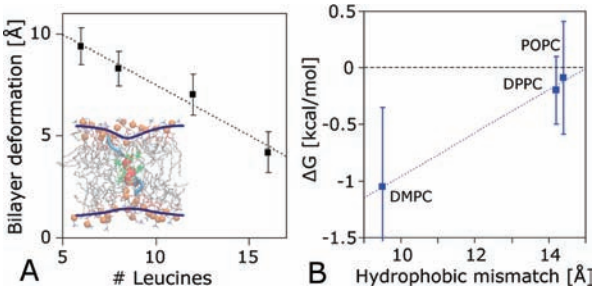

Figure 9. The role of bilayer thickness and deformation on shifting the partitioning equilibrium. (A) Peptide induced bilayer deformation for GLn (n = 6−16) sequences in their TM-inserted orientation. The deformation rises with increased negative hydrophobic mismatch. (Inset: GL8, the thick line indicating the average position of the phosphate groups). (B) The partitioning equilibrium is shifted toward the TM orientation upon decreasing the bilayer thickness due to a reduced hydrophobic mismatch.

hydrophobic core prohibits insertion. Consequently, the flanking sequences remain in the polar lipid headgroup region throughout the simulations, either with both flanks at the same interface (S state), or one on each side of the bilayer (TM state). The net contribution to the insertion propensities is $\Delta\Delta G^{\text{flanks}}_{\text{S}\rightarrow\text{TM}} \approx 0$ ($\Delta G^{\text{L}n}_{\text{S}\rightarrow\text{TM}} \approx \Delta G^{\text{GL}n}_{\text{S}\rightarrow\text{TM}}$). Interestingly, similar observations were made in the translocon experiments: adding additional glycines to the GPGG flanks had an almost negligible effect, with free energy shifts of $\Delta\Delta G$ = +0.18 kcal/mol for GPGGG to −0.17 kcal/mol for GPGGGGGG. Substituting all Gly residues with Asn led to only a small increase of $\Delta\Delta G$ = +0.5 kcal/mol. Hence, $\Delta G^{\text{flanks}}_{\text{exp}} \approx 0$. This is consistent with our simulations: flanking sequences are not inserted into the bilayer core and thus do not contribute to $\Delta G_{\text{S}\rightarrow\text{TM}}$. Flanking sequences have, however, a dramatic effect on the insertion barriers. For TM insertion and expulsion, a flanking tetrapeptide has to be translocated from one interface across the bilayer core to the other. We find a barrier of $\Delta H^{\ddagger}_{\text{S}\leftrightarrow\text{TM}}$ = 20−24 kcal/mol per GPGG flank or ∼5−6 kcal/mol per flanking residue. This compares well with previous estimates for the transfer of an unmatched hydrogen bonding pair into alkane of ∼6.4 kcal/mol.[26] Without flanks, the peptide partitioning barrier is significantly reduced to $\Delta H^{\ddagger}_{\text{S}\leftrightarrow\text{TM}}$ = 5.5−8.1 kcal/mol.

In order to investigate whether the simulation results depend on the hydrophobic thickness of the bilayer, we performed control simulations of the L7 peptide in bilayers composed of lipids with different acyl lengths. The results, for DPPC and DMPC, are shown in Figure 9, Figure S2 (Supporting Information), and Table 2. ΔG is very similar for POPC and DPPC, indicating that the acyl chain saturation plays only a minor role. However, the partitioning equilibrium is shifted by −0.9 kcal/mol toward the TM state in the DMPC bilayer, demonstrating that bilayer thickness greatly affects the insertion free energy. This effect is caused by the energetic cost of membrane deformation, which is lower in thinner membranes as the hydrophobic mismatch is reduced (Figure 9).[8,30] However, as the thickness of the POPC bilayer is comparable to that of the ER membrane,[8,31,32] this is unlikely to be the cause of the shift between experimental and simulated insertion.

Another surprising result is the apparent temperature-insensitivity of $\Delta G_{\text{S}\rightarrow\text{TM}}$ (Figure 7, Figure 8). Given the ∼10% uncertainties of both p_{TM} and $\Delta G_{\text{S}\rightarrow\text{TM}}$, several thermodynamic

Table 2. Influence of the Lipid Environment on the Partitioning Properties[a]

	POPC	DPPC	DMPC
hydrophobic thickness (Å)	27.7[b]	27.9[c]	23[d]
hydrophobic mismatch (Å)	−14.2	−14.4	−9.5
p_{insert} (%)	58 ± 9	53 ± 16	82 ± 13
ΔG_{insert} (kcal/mol)	−0.2 ± 0.3	−0.09 ± 0.5	−1.05 ± 0.7

[a] The results are for simulations of L7 at 80 °C. The hydrophobic mismatch is defined as the difference between the length of the peptide and the hydrophobic thickness of the lipid bilayers. It is assumed that each amino acid has a length of 1.5 Å. With the terminal capping groups included, this yields 13.5 Å for an ideal TM-inserted α-helix. [b] Reference 32. [c] Reference 33. [d] Reference 34.

models could be fitted to the data. We found the best match for $\Delta G(T)_{\text{S}\rightarrow\text{TM}} \approx$ constant, and $p_{\text{TM}} = [1 + \exp(-\beta\Delta G_{\text{S}\rightarrow\text{TM}})]^{-1}$, as illustrated in Figure 8. Using $\Delta G_{\text{S}\rightarrow\text{TM}} = \Delta H_{\text{S}\rightarrow\text{TM}} - T\Delta S_{\text{S}\rightarrow\text{TM}}$ and assuming only a small explicit dependence of ΔH and ΔS on T, this implies that $\Delta S_{\text{S}\rightarrow\text{TM}} \approx 0$. Why do entropic effects play only a minor role? First, the peptides do not unfold (see thermostability, Figure 5A,B), and thus there are no entropic contributions from conformational changes. Second, the entropic penalty $\Delta S_{\text{immobilize}}$ on immobilizing the peptide inside the membrane[35] arising from the restriction of the rigid body rotational (e.g., tilting) and translational motions (e.g., diffusion along the membrane normal) is identical for the S and TM states: for example, the center of mass and tilt angle fluctuations of GL8 are ±1.9 Å/±10.1° for the TM, and ±2.1 Å/±11.1° for the S state. Third, upon heating there is a notable 5−10% decrease in both the membrane density and thickness (Figure 5C). Nevertheless, this does not affect the relative positions of the individual structural groups along the membrane normal, and the overall transbilayer chemical profile is retained. Furthermore, both TM and S helices remain deeply buried inside the hydrophobic phase and are thus affected in the same way. While a model where $\Delta S_{\text{S}\rightarrow\text{TM}} \approx 0$ fits the data well, assuming $\Delta H_{\text{S}\rightarrow\text{TM}} \approx$ constant neglects changes in heat capacity. It is likely that small nonvanishing entropic contributions exist, and both $\Delta H(T)$ and $\Delta S(T)$ are temperature dependent. However, the large statistical uncertainties in ΔG at low temperatures (e.g., ∼25% at 30 °C), as well as the very large errors for direct estimates of $\Delta H_{\text{S}\rightarrow\text{TM}}$ unfortunately prevent a more rigorous analysis of the temperature dependence.

In addition to converged insertion propensities, the direct simulation protocol is well suited to obtain quickly the transition rates at ambient temperatures by extrapolation of the observed single-exponential kinetics. This is very useful, because the insertion times at 30 °C can be much longer than the lengths presently obtainable in MD simulation (e.g., ∼200 ms for GL8, see Table 2).[36] On the other hand, the simulations of L7 and L8 demonstrate that in cases where the barriers are weak (∼5−8 kcal/mol), multiple transition events can be obtained within ∼1 μs at 30 °C, and high temperatures are not required.

The most puzzling result of our study is the close correlation between the spontaneous surface-to-bilayer partitioning equilibrium and the translocon-mediated insertion scale; the plots of free energy versus the number of leucines have similar slopes but are offset (Figure 7B). The results show that ∼2 fewer leucines are required for the peptides to insert on their own than predicted by the translocon scale. The probable explanation is that

two different partitioning processes are involved. In contrast to partitioning between bilayer interface and hydrocarbon core, the translocon crystal structure suggests that hydrophobic peptides are released laterally from the protein conducting channel into the membrane.[37] This means that the experiments measure the partitioning of peptides between translocon channel and bilayer, rather than between water-soluble and TM configurations (Figure 1B).[7,11−14] Experimental support for this interpretation comes from a recent mutagenesis study by Junne et al. in which an increase in polarity of the Sec61 translocon protein conducting channel was found to reduce drastically the minimal peptide hydrophobicity required for membrane insertion.[10] This is consistent with a translocon-to-bilayer equilibrium being at the heart of the translocon-mediated insertion probability. Recently, Gumbart et al. have performed simulations that seem to confirm this view:[38] The transfer free energies from the translocon to the membrane were found to be significantly smaller than those of water-to-bilayer transfer and more in line with the translocon experiments. Thus, the close correlation of our results indicates that the surface-bound helical state of the peptides is located in a region of hydrophobicity similar to that of the internal translocon pore. This suggests that the equilibria of spontaneous partitioning and translocon-mediated insertion are likely independent, with no thermodynamic cycle connecting the two insertion paths, as recently discussed.[7] Both differ highly from the much larger free energy changes involved in nonequilibrium water-to-bilayer partitioning.

The direct partitioning simulations presented here are completely general and can be readily adapted to study any peptide, regardless of the sequence, including polar and charged peptides. As an equilibrium approach, it can quickly detect all relevant equilibrium states available to the peptide in the presence of a lipid bilayer, provided they are thermally accessible. For the hydrophobic sequences presented here, this equilibrium is purely between a surface and a TM-inserted state. This is in agreement with the experimental fact that these peptides are insoluble. Gumbart et al. have estimated that for a polyleucine helix, the water solvated state is ∼56 kcal/mol higher in free energy, which would correspond to a population difference of $1/10^{35}$.[38] However, if the peptide is charged and more water-soluble, the water state will become accessible and populated, and the equilibrium will instead be between water and the bilayer surface. Thus, conventional equilibrium simulations can also be applied to charged and polar peptides. For the specific case of obtaining peptide−bilayer partitioning free energies, equilibrium simulations offer an alternative to potential of mean force (PMF) calculations, which can be challenging, as recently demonstrated for polyleucine.[38]

The direct approach presented here thus constitutes a simple, efficient, and general tool to determine single molecule partitioning properties as well as transfer kinetics of peptides into lipid bilayers. This speeds up investigations of the insertion mechanism of membrane active peptides (e.g., antimicrobials, cell-penetrating, and fusion peptides), or de novo membrane protein structure prediction via ab initio folding−partitioning and assembly simulations at an increased level of structural and dynamic detail.

METHODS

Experiments. GL12 was solid-state synthesized using standard FMOC chemistry and purified using HPLC. The peptide was incorporated into DPPC lipid vesicles using the dry film method. CD spectra were recorded on a Jasco J-720 spectropolarimeter, using a 1 mm path length quartz cuvette. The peptide concentration was 30 μM, and the molar peptide/lipid ratio was 1/100. Temperature was controlled with a Peltier device and varied between 20 °C and 90 °C in 5 °C steps. Samples were equilibrated for 5 min at each temperature, and measurements were repeated five times. All spectra were corrected for background scattering by subtracting the corresponding vesicle-only spectrum measured over the same temperature range (see Supporting Information for details).

Simulations. Simulations were performed using Gromacs 4.0 (www.gromacs.org),[39] and analysis was performed with Hippo beta (www.biowerkzeug.com). All systems were simulated in the NPT ensemble using the OPLS all-atom (OPLS-AA) protein force field[40] in combination with the TIP3P water model,[41] and OPLS-AA-compatible united-atom lipid parameters were recently parametrized by us.[42] Atmospheric pressure of 1 bar was applied, and the temperature range was 30 °C to 217 °C (see Supporting Information for details).

ASSOCIATED CONTENT

Supporting Information. Further details on the computational and experimental methods, and a list of all simulations performed as well as additional analysis. This material is available free of charge via the Internet at http://pubs.acs.org.

AUTHOR INFORMATION

Corresponding Author
jakob@ulmschneider.com; martin@ulmschneider.com

ACKNOWLEDGMENT

This research was supported by a Marie Curie International Fellowship to M.B.U, by a Center for Modeling and Simulation in the Biosciences Fellowship to J.P.U., by grants from the National Institute of General Medical Science and the National Institute of Neurological Disorders to S.H.W., and a Laboratory Directed Research and Development award from the U.S. Department of Energy to J.C.S.

REFERENCES

(1) Ladokhin, A. S.; White, S. H. *Biochemistry* **2004**, *43*, 5782–5791.
(2) Wimley, W. C.; White, S. H. *Biochemistry* **2000**, *39*, 4432–4442.
(3) Hessa, T.; Kim, H.; Bihlmaier, K.; Lundin, C.; Boekel, J.; Andersson, H.; Nilsson, I.; White, S. H.; von Heijne, G. *Nature* **2005**, *433*, 377–381.
(4) Hessa, T.; Meindl-Beinker, N. M.; Bernsel, A.; Kim, H.; Sato, Y.; Lerch-Bader, M.; Nilsson, I.; White, S. H.; von Heijne, G. *Nature* **2007**, *450*, 1026–1030.
(5) Hessa, T.; White, S. H.; von Heijne, G. *Science* **2005**, *307*, 1427.
(6) Wimley, W. C.; Creamer, T. P.; White, S. H. *Biochemistry* **1996**, *35*, 5109–5124.
(7) Schow, E.; Freites, J.; Cheng, P.; Bernsel, A.; von Heijne, G.; White, S.; Tobias, D. *J. Membr. Biol.* **2011**, *239*, 35–48.
(8) Jaud, S.; Fernández-Vidal, M.; Nillson, I.; Meindl-Beinker, N. M.; Hübner, N. C.; Tobias, D. J.; von Heijne, G.; White, S. H. *Proc. Natl. Acad. Sci. U.S.A.* **2009**, *106*, 11588–11593.
(9) Ulmschneider, M. B.; Doux, J. P. F.; Killian, J. A.; Smith, J.; Ulmschneider, J. P. *J. Am. Chem. Soc.* **2010**, *132*, 3452–3460.
(10) Junne, T.; Kocik, L.; Spiess, M. *Mol. Biol. Cell* **2010**, *21*, 1662–1670.
(11) Von Heijne, G. *J. Gen. Physiol.* **2007**, *129*, 353–356.
(12) White, S. H. *J. Gen. Physiol.* **2007**, *129*, 363–369.

(13) White, S. H.; von Heijne, G. *Biochem. Soc. Trans.* **2005**, *33*, 1012–5.
(14) White, S. H.; von Heijne, G. *Curr. Opin. Struct. Biol.* **2005**, *15*, 378–386.
(15) White, S. H.; Wimley, W. C. *Annu. Rev. Biophys. Biomol. Struct.* **1999**, *28*, 319–365.
(16) Engelman, D. M.; Chen, Y.; Chin, C.-N.; Curran, A. R.; Dixon, A. M.; Dupuy, A. D.; Lee, A. S.; Lehnert, U.; Matthews, E. E.; Reshetnyak, Y., K.; Senes, A.; Popot, J.-L. *FEBS Lett.* **2003**, *555*, 122–125.
(17) Sugita, Y.; Okamoto, Y. *Chem. Phys. Lett.* **1999**, *314*, 141–151.
(18) Nymeyer, H.; Woolf, T. B.; Garcia, A. E. *Proteins: Struct. Funct. Bioinf.* **2005**, *59*, 783–790.
(19) Ulmschneider, J. P.; Ulmschneider, M. B. *J. Chem. Theory Comput.* **2007**, *3*, 2335–2346.
(20) Ulmschneider, J. P.; Ulmschneider, M. B. *Proteins: Struct. Funct. Bioinf.* **2009**, *75*, 586–597.
(21) Ulmschneider, J. P.; Ulmschneider, M. B.; Di Nola, A. *J. Phys. Chem. B* **2006**, *110*, 16733–16742.
(22) Ulmschneider, J. P.; Ulmschneider, M. B.; Di Nola, A. *Proteins: Struct. Funct. Bioinf.* **2007**, *69*, 297–308.
(23) Ulmschneider, M. B.; Ulmschneider, J. P.; Sansom, M. S. P.; Di Nola, A. *Biophys. J.* **2007**, *92*, 2338–2349.
(24) Im, W.; Brooks, C. L. *Proc. Natl. Acad. Sci. U.S.A.* **2005**, *102*, 6771–6776.
(25) Ladokhin, A. S.; White, S. H. *J. Mol. Biol.* **1999**, *285*, 1363–1369.
(26) Ben-Tal, N.; Sitkoff, D.; Topol, I. A.; Yang, A.-S.; Burt, S. K.; Honig, B. *J. Phys. Chem. B* **1997**, *101*, 450–457.
(27) Pabst, G.; Katsaras, J.; Raghunathan, V. A. *Phys. Rev. Lett.* **2002**, *88*, 128101.
(28) de Pablo, J. J.; Prausnitz, J. M.; Strauch, H. J.; Cummings, P. T. *J. Chem. Phys.* **1990**, *93*, 7355–7359.
(29) Frenkel, D.; Smit, B. *Understanding Molecular Simulation*, 2nd ed.; Academic Press, Inc.: Orlando, FL, 2001.
(30) Krishnakumar, S. S.; London, E. *J. Mol. Biol.* **2007**, *374*, 671–87.
(31) Mitra, K.; Ubarretxena-Belandia, I.; Taguchi, T.; Warren, G.; Engelman, D. M. *Proc. Natl. Acad. Sci. U.S.A.* **2004**, *101*, 4083–4088.
(32) Gawrisch, K.; Gaede, H. C.; Mihailescu, M.; White, S. H. *Eur. Biophys. J.* **2007**, *36*, 281–291.
(33) Kucerka, N.; Tristram-Nagle, S.; Nagle, J. F. *Biophys. J.* **2006**, *90*, L83−L85.
(34) Lewis, B. A.; Engelman, D. M. *J. Mol. Biol.* **1983**, *166*, 211–217.
(35) Ben-Tal, N.; Ben-Shaul, A.; Nicholls, A.; Honig, B. *Biophys. J.* **1996**, *70*, 1803–1812.
(36) Meijberg, W.; Booth, P. J. *J. Mol. Biol.* **2002**, *319*, 839–853.
(37) Van den Berg, B.; Clemons, W. M., Jr.; Collinson, I.; Modis, Y.; Hartmann, E.; Harrison, S. C.; Rapoport, T. A. *Nature* **2004**, *427*, 36–44.
(38) Gumbart, J.; Chipot, C.; Schulten, K. *Proc. Natl. Acad. Sci. U.S.A.* **2011**, *108*, 3596–3601.
(39) Berendsen, H. J. C.; van der Spoel, D.; van Drunen, R. *Comput. Phys. Commun.* **1995**, *91*, 43–56.
(40) Jorgensen, W. L.; Maxwell, D. S.; Tirado-Rives, J. *J. Am. Chem. Soc.* **1996**, *118*, 11225–11236.
(41) Jorgensen, W. L.; Chandrasekhar, J.; Madura, J. D.; Impey, R. W.; Klein, M. L. *J. Chem. Phys.* **1983**, *79*, 926–935.
(42) Ulmschneider, J. P.; Ulmschneider, M. B. *J. Chem. Theory Comput.* **2009**, *5*, 1803–1813.